Journal of Sound and Vibration (2001) **244**(5), 779–793
doi:10.1006/jsvi.2000.3537, available online at http://www.idealibrary.com on IDEAL®

DYNAMIC INSTABILITY REGIONS IN A DAMPED SYSTEM

I. SVENSSON

Division of Solid Mechanics, Lund University, Box 118, *S*-221 00 *Lund, Sweden.*
E-mail: Ingrid@solid.lth.se

(*Received* 8 *May* 2000, *and in final form* 15 *November* 2000)

The stability properties of a periodically loaded non-linear dynamic system are investigated and special attention is given to damping effects. Advantage is taken of the Floquet theory and the FE-approach is applied to a hinged beam where the damping is described by a standard material model and where even damping effects at the hinges are considered. Comparisons are made with experimental results.

1. INTRODUCTION

In many engineering systems of practical importance, one encounters excited systems which exhibit periodic, aperiodic or even chaotic behaviour depending on the loading parameters (see, e.g., references [1–4]). The principal issue which has to be solved is the question of stability of the system, reduced in many cases to the problem of finding the stability conditions of a particular solution. However, to solve the general problem, that is, to identify the stability borders in the complete loading parameter space for a periodically excited system, is a more complex issue. One way is to use Floquet theory and perform a numerical integration of the governing differential equations from the initial value equal to the identity matrix, over the time corresponding to one time period of the loading to establish the transition or monodromie matrix [5]. The stability properties of the solution are then given by examination of the eigenvalues of the monodromie matrix. To determine the stable and unstable regions in the loading parameter space with this approach, one has to establish a gridwork and do the numerical integration for each nodal point in that gridwork. This is an inefficient method; instead, advantage is taken of the fact that at that stability borders in the loading parameter space, the solutions of the system become periodic. This is a conclusion of the Floquet theory and, thanks to the periodicity, the solutions can be expressed as Fourier series. From the Fourier expansions, the stability borders are given by the solution of an eigenvalue problem of infinite order. An approximation is achieved by taking the first order subdeterminant of the matrices of coefficients; this technique is adopted originally in reference [6] and later on in, for example, reference [7]. The same technique combined with FE-formulation is used in reference [8] and there the periodic loading term gives an extra contribution to the stiffness matrix. In reference [9], a finite difference method is used for deriving the instability regions for clamped–clamped and clamped–simply supported columns under periodic axial loading. The investigation is complemented by experimental results.

If a dynamic system is to be described, the question of how to deal with damping always appears. Damping is often crucial when dealing with stability problems, both for describing the stable or unstable motion of the system and when the stability borders in the parameter

0022-460X/01/300779 + 15 $35.00/0

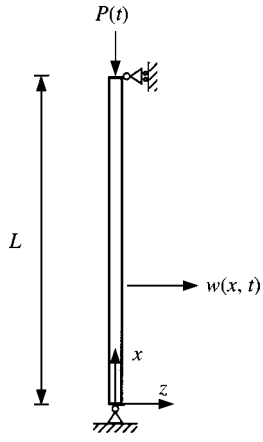

Figure 1. The system under study.

space are to be determined. Here, a computation model including external damping in the boundary conditions and internal material effects is established. The starting point is a rather general material model which will cause third order time derivatives in the governing equations. However, the concept of the Fourier expansions of the solutions at the stability borders can still be used. In the FE-formulation, boundary terms governing damping are included and the method will be illustrated by calculating the stability diagram of an axially loaded beam in an efficient way. It might seem to be more complicated than is necessary when using FE-elements for a geometry where the global modes are already known [6]. However, this system is chosen just for illustration and the method presented can be used for systems with more complicated boundary conditions and elastic frameworks. The calculations are performed in Matlab using the FE tool-box CALFEM [10] and the influence of both material damping and damping at the boundary will be verified experimentally.

2. INVESTIGATED SYSTEM

The system considered is a homogeneous transversally vibrating beam with length L, constant cross-section A and mass density ρ. The beam is loaded axially with the force $P(t)$ (positive in compression) and $w(x, t)$ is the transverse deflection of the beam midpoint (Figure 1).

2.1. EQUATIONS OF MOTION

The general expression of virtual work is stated as

$$\int_V \sigma_{ij}\delta\varepsilon_{ij}\,\mathrm{d}V = \int_V (F_i - \rho\ddot{u}_i)\delta u_i\,\mathrm{d}V + \int_S t_i\delta u_i\,\mathrm{d}S, \tag{1}$$

where σ_{ij} and ε_{ij} denote the stress and strain tensors, respectively, V is the region and S is the boundary surface of the region. Moreover, u_i is the displacement vector and a dot denotes differentiation with respect to time. The loading terms are given the body force vector per

unit volume F_i and the surface traction vector t_i. Adopting the Euler–Bernoulli assumption for the beam, the displacements u_i are

$$\begin{aligned} u_1 &= u - z\frac{\partial w}{\partial x}, \\ u_2 &= 0, \\ u_3 &= w, \end{aligned} \tag{2}$$

where $u(x, t)$ is the longitudinal displacement measured positively in the x direction (Figure 1). In this work, the von Karman assumption [11] is used, allowing Green's normal strain tensor ε along the beam axis to be approximated as

$$\varepsilon \approx \frac{\partial u_1}{\partial x} + \frac{1}{2}\left(\frac{\partial u_3}{\partial x}\right)^2 = \frac{\partial u}{\partial x} - z\frac{\partial^2 w}{\partial x^2} + \frac{1}{2}\left(\frac{\partial w}{\partial x}\right)^2. \tag{3}$$

Note that due to the Euler–Bernoulli assumption only the normal strain (3) is assumed to exist.

With these definitions and in the absence of the body forces F_i, equation (1) can be written as

$$\begin{aligned} &\int_V \sigma\left(\frac{\partial \delta u}{\partial x} - z\frac{\partial^2 \delta w}{\partial x^2} + \frac{\partial \delta w}{\partial x}\frac{\partial w}{\partial x}\right)\mathrm{d}V \\ &= -\rho\int_V \left(\ddot{u}\delta u - z\ddot{u}\frac{\partial \delta w}{\partial x} - z\frac{\partial \ddot{w}}{\partial x}\delta u + z^2\frac{\partial \ddot{w}}{\partial x}\frac{\partial \delta w}{\partial x} + \ddot{w}\delta w\right)\mathrm{d}V \\ &\quad + \int_S \left(t_1\delta u - z t_1\frac{\partial \delta w}{\partial x} + t_3\delta w\right)\mathrm{d}S, \end{aligned} \tag{4}$$

where $\sigma = \sigma_{11}$ is the normal stress. To reduce the above equation to a more convenient form, the volume integrals are split into an integral along the beam axis and an integral over the cross-section. Moreover, it also turns out to be advantageous to locate the beam axis at the mass centre of the cross-section, i.e., $\int_A z\,\mathrm{d}A = 0$ where A is the cross-section of the beam.

From the split of the first volume integral it then follows that the section resultants

$$N = \int_A \sigma\,\mathrm{d}A \quad \text{and} \quad M = \int_A z\sigma\,\mathrm{d}A \tag{5}$$

are natural quantities, where N is the normal force and M is the bending moment. The moment of inertia I of the cross-section is defined by

$$I = \int_A z^2\,\mathrm{d}A, \tag{6}$$

whereas the transverse shear force Q is defined by

$$Q = \int_A \sigma_3\,\mathrm{d}A. \tag{7}$$

Considering loading only at the endpoints of the beam, it follows that the surface integral in equation (4) is identical to the cross-section integral, i.e., $\mathrm{d}S = \mathrm{d}A$. Moreover, from $t_i = \sigma_{ij} n_j$ where n_j is the unit normal vector pointing out from the body, it is found that at $x = 0$, $t_1 = -\sigma_{11}$ and $t_3 = -\sigma_{31}$ and at $x = L$, $t_1 = \sigma_{11}$ and $t_3 = \sigma_{31}$. Finally, using equations (5) and (6) in equation (4) gives

$$\int_x N\left(\frac{\partial \delta u}{\partial x} + \frac{\partial w}{\partial x}\frac{\partial \delta w}{\partial x}\right)\mathrm{d}x - \int_x M\frac{\partial^2 \delta w}{\partial x^2}\,\mathrm{d}x = -\rho A\int_x (\ddot{u}\delta u + \ddot{w}\delta w)\,\mathrm{d}x$$

$$-\rho I\int_x \frac{\partial \ddot{w}}{\partial x}\frac{\partial \delta w}{\partial x}\,\mathrm{d}x + \left[\delta u\, N + \delta w\, Q - \frac{\partial \delta w}{\partial x}M\right]_0^L. \tag{8}$$

After partial integrations of selected terms knowing that δu can be varied arbitrarily, the equation of motion in the x direction is given as

$$-\frac{\partial N}{\partial x} + \rho A\ddot{u} = 0 \tag{9}$$

and by varying δw it follows that

$$-\frac{\partial^2 M}{\partial x^2} - \frac{\partial}{\partial x}\left(N\frac{\partial w}{\partial x}\right) - \rho I\frac{\partial^2 \ddot{w}}{\partial x^2} + \rho A\ddot{w} = 0. \tag{10}$$

Moreover, the natural boundary condition associated with the problem formulation is

$$Q = \frac{\mathrm{d}M}{\mathrm{d}x} + N\frac{\partial w}{\partial x} + \rho I\frac{\partial \ddot{w}}{\partial x}. \tag{11}$$

The third term in equation (10) governs the effect of the rotary inertia and can be ignored for the problem in question [4]. Then the third term in the boundary condition for the force Q in equation (11) will vanish.

If the axial force is assumed to oscillate sinusoidally with time, cf. equation (22), and the period of oscillation, $2\pi/\omega$, is at least one order of magnitude higher than the travel time of longitudinal waves from one end of the beam to the other, then the longitudinal wave motion can be neglected. Consequently, the normal force is not dependent upon the position along the beam and $N \simeq -P$.

2.2. MATERIAL MODEL

Two different types of damping will be considered in this paper, material damping and damping at the boundaries. Here a derivation of the material damping will be given in a thermodynamic framework described in reference [12]. To obtain a viscoelastic material model it is assumed that the total strain ε can be split into an elastic part, ε^e, and a viscous part ε^v, i.e.,

$$\varepsilon = \varepsilon^e + \varepsilon^v. \tag{12}$$

Since isothermal conditions are considered, the second law of thermodynamics written as Clausius–Duhem's inequality takes the form

$$\gamma = \sigma\dot{\varepsilon} - \rho\dot{\psi}(\varepsilon, \varepsilon^v) \geqslant 0, \tag{13}$$

where γ is the dissipation function and ψ denotes Helmholtz's free energy function per unit mass. The specific form of Helmholtz's free energy function is taken as

$$\rho\psi(\varepsilon, \varepsilon^v) = \tfrac{1}{2}(\varepsilon - \varepsilon^v)E(\varepsilon - \varepsilon^v) + \frac{\bar{E}}{2}\varepsilon_v^2. \tag{14}$$

Here, E is the modulus of elasticity and $\bar{E}$ a hardening modulus. Making use of equation (14) in equation (13) yields

$$\gamma = \left(\sigma - \rho\frac{\partial\psi}{\partial\varepsilon}\right)\dot{\varepsilon} - \rho\frac{\partial\psi}{\partial\varepsilon^v}\dot{\varepsilon}^v \geqslant 0. \tag{15}$$

Since this inequality should hold for all $\dot{\varepsilon}$ and $\dot{\varepsilon}^v$, an allowable solution is given by

$$\gamma = -\sigma^v\dot{\varepsilon}^v \geqslant 0 \tag{16}$$

and

$$\begin{aligned} \sigma &= \rho\frac{\partial\psi}{\partial\varepsilon} = E(\varepsilon - \varepsilon^v), \\ \sigma^v &= \rho\frac{\partial\psi}{\partial\varepsilon^v} = -\sigma + \bar{E}\varepsilon^v. \end{aligned} \tag{17}$$

To satisfy the dissipation inequality the evolution law for $\dot{\varepsilon}^v$ is taken as

$$\dot{\varepsilon}^v = -\mu\sigma^v, \tag{18}$$

where μ is the viscosity parameter of the material. Using equation (18) in equation (16) then yields $\gamma = \mu(\sigma^v)^2 \geqslant 0$, that is, it is necessary that $\mu \geqslant 0$ to satisfy the second law of thermodynamics.

Solving ε^v from equation (17a) and insertion into equation (17b) gives

$$\sigma^v = \bar{E}\varepsilon - \left(1 + \frac{\bar{E}}{E}\right)\sigma. \tag{19}$$

The stress–strain relation is then found by a differentiation of equation (17a) and use of equations (18) and (19) to obtain

$$\dot{\sigma} + \mu(E + \bar{E})\sigma = \mu\bar{E}E\varepsilon + E\dot{\varepsilon}. \tag{20}$$

The above stress–strain law is known as a standard material model. If $\mu = 0$ usual elasticity is found, if $\bar{E} = 0$ a Maxwell material model is obtained and if $E \to \infty$ a Kelvin model is obtained. In the latter case, however, the thermodynamic arguments leading to equation (20) need, in principle, to be modified and a dissipative stress must be introduced in equation (17a). Making use of the definition of the strain tensor, cf. equation (3), multiplying equation (20) by z and integrating over the cross-section area it follows that equation (20) can be written as

$$\dot{M} + \mu(E + \bar{E})M = -\mu\bar{E}EI\frac{\partial^2 w}{\partial x^2} - EI\frac{\partial^2\dot{w}}{\partial x^2}, \tag{21}$$

where equations (6) and (5b) were used.

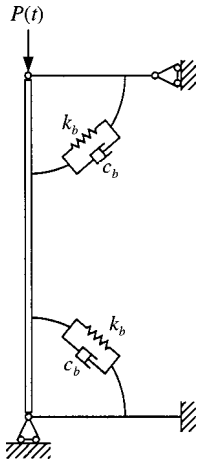

Figure 2. The hinges.

3. STRONG FORM OF THE EQUATION OF MOTION

The driving force in the system is given by the axial force $P(t)$ (Figure 1), which is assumed to vary harmonically with time, i.e.,

$$P = P(t) = P_S + P_D \cos \omega t. \tag{22}$$

First, derive the equation of motion (10) in terms of the transverse deflection where, as previously mentioned, the rotary inertia term can be ignored. Differentiation of equation (21) with respect to the position co-ordinate x twice and using equation (10) as well as $N = -P$ results in

$$\mu \bar{E} EI \frac{\partial^4 w}{\partial x^4} + EI \frac{\partial^4 \dot{w}}{\partial x^4} + [\mu(E + \bar{E})P + \dot{P}] \frac{\partial^2 w}{\partial x^2} + P \frac{\partial^2 \dot{w}}{\partial x^2} + \rho A \ddot{w} + \mu(E + \bar{E}) \rho A \ddot{w} = 0. \tag{23}$$

To finally settle the strong form of the problem the boundary conditions must be specified. The boundary conditions are introduced here in such a way that not only flexibility, but also damping can be accounted for. Therefore, the hinges are modelled by one stiffness part and one viscous part; i.e.,

$$M_{(x=0)} = -\left[k_b \frac{\partial w}{\partial x} + c_b \frac{\partial \dot{w}}{\partial x} \right]_{(x=0)}, \quad M_{(x=L)} = \left[k_b \frac{\partial w}{\partial x} + c_b \frac{\partial \dot{w}}{\partial x} \right]_{(x=L)}. \tag{24}$$

Obviously, stiff hinges can be modelled by letting $k_b \to \infty$, and free hinges by $k_b = c_b = 0$ (Figure 2). Finally, the essential boundary conditions are given as $w(0) = w(L) = 0$.

3.1. FE-FORMULATION

The FE-formulation is obtained in a standard manner, i.e., the strong form of the equation of motion (23) is multiplied with an arbitrary weight function $v(x)$, integrated over

the length of the beam and selected terms are integrated by parts twice, thereby arriving at the weak form. Moreover, the approximation for w is introduced as

$$w(x, t) = \mathbf{N}(x)\mathbf{a}(t), \tag{25}$$

where $\mathbf{N}(x)$ are the global shape functions and $\mathbf{a}(t)$ is the nodal displacement vector. Moreover,

$$\frac{\partial^2 w}{\partial x^2} = \mathbf{B}(x)\,\mathbf{a}(t), \quad \mathbf{B} = \frac{\mathrm{d}^2\mathbf{N}}{\mathrm{d}x^2}. \tag{26}$$

Following Galerkin's method, the weight vector is approximated with the same shape functions, i.e.,

$$v = \mathbf{N}(x)\mathbf{c} = \mathbf{c}^{\mathrm{T}}\mathbf{N}^{\mathrm{T}}, \quad \frac{\partial^2 v}{\partial x^2} = \mathbf{B}\mathbf{c} = \mathbf{c}^{\mathrm{T}}\mathbf{B}^{\mathrm{T}}. \tag{27}$$

In the following evaluation, shape functions are chosen which approximate the deflection as a Hermite interpolation. Inserting these approximations in the weak form of equation (23), using the relations of equations (24) for the boundary terms and noting that the **c**-matrix is independent of the co-ordinate x, will result in the Mathieu differential equation (23) written in matrix format as

$$\mathbf{M}^*\dddot{\mathbf{a}} + \mathbf{M}\ddot{\mathbf{a}} + (\mathbf{C} + \mathbf{K}_{gS} + \mathbf{K}_{gD}\cos\omega t)\,\dot{\mathbf{a}} + (\mathbf{K}_e + \mu(E + \bar{E})(\mathbf{K}_{gS} + \mathbf{K}_{gD}\cos\omega t) - \omega\mathbf{K}_{gD}\sin\omega t)\,\mathbf{a} = \mathbf{0}, \tag{28}$$

where

$$\begin{aligned}
\mathbf{K}_e &= \int_0^L \mathbf{B}^{\mathrm{T}}\mu\bar{E}EI\mathbf{B}\,\mathrm{d}x - \left[\frac{\mathrm{d}\mathbf{N}^{\mathrm{T}}}{\mathrm{d}x}\,\mu(E + \bar{E})k_b\,\frac{\mathrm{d}\mathbf{N}}{\mathrm{d}x}\right]_0^L,\\
\mathbf{K}_{gS} &= \int_0^L \frac{\mathrm{d}\mathbf{N}^{\mathrm{T}}}{\mathrm{d}x}(-P_S)\frac{\mathrm{d}\mathbf{N}}{\mathrm{d}x}\,\mathrm{d}x,\\
\mathbf{K}_{gD} &= \int_0^L \frac{\mathrm{d}\mathbf{N}^{\mathrm{T}}}{\mathrm{d}x}(-P_D)\frac{\mathrm{d}\mathbf{N}}{\mathrm{d}x}\,\mathrm{d}x,\\
\mathbf{C} &= \int_0^L \mathbf{B}^{\mathrm{T}}EI\mathbf{B}\,\mathrm{d}x - \left[\frac{\mathrm{d}\mathbf{N}^{\mathrm{T}}}{\mathrm{d}x}(k_b + \mu(E + \bar{E})c_b)\frac{\mathrm{d}\mathbf{N}}{\mathrm{d}x}\right]_0^L,\\
\mathbf{M} &= \mu(E + \bar{E})\int_0^L \mathbf{N}^{\mathrm{T}}\rho A\mathbf{N}\,\mathrm{d}x - \left[\frac{\mathrm{d}\mathbf{N}^{\mathrm{T}}}{\mathrm{d}x}\,c_b\,\frac{\mathrm{d}\mathbf{N}^{\mathrm{T}}}{\mathrm{d}x}\right]_0^L,\\
\mathbf{M}^* &= \int_0^L \mathbf{N}^{\mathrm{T}}\rho A\mathbf{N}\,\mathrm{d}x.
\end{aligned} \tag{29}$$

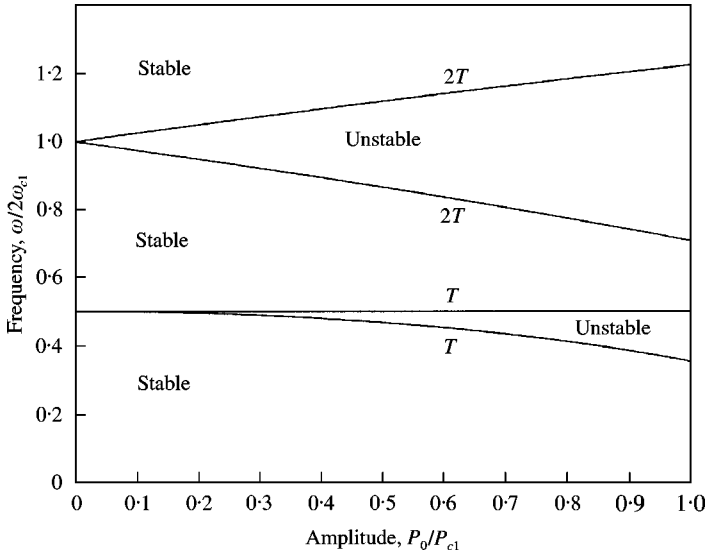

Figure 3. Stability chart of the undamped simply supported system. The load scale is normalized with the first buckling load and the frequency scale is normalized with two times the lowest eigenfrequency.

In the FE-formulation (28), advantage has already been taken of the essential boundary conditions, i.e., $w(0) = w(L) = 0$.

Equation (28), in which some coefficients change harmonically, is recognized as a Mathieu differential equation in matrix form. From the theory of Mathieu functions [13, 6], it is evident that the nature of the solution is dependent on the choice of load frequency and load amplitude. The frequency–amplitude domain is divided into regions which give rise to stable solutions and to regions which cause unstable solutions. On the border lines between the stable and unstable regions, the solutions are periodic with period $T = 2\pi/\omega$ or $2T$; this follows from the theory of Floquet [6]. More precisely, two solutions of identical periodicity bound the region of instability and two solutions of different periodicity bound the region of stability (Figure 3). In this context, a stable solution means that the motions remain within a bounded neighbourhood of the initial conditions, i.e., stability in the Lyapunov sense [14].

4. PRELIMINARIES

Since the solutions of equation (28) are periodic on the stability border lines, it seems natural to express them as trigonometric time series expansions, i.e.,

$$\text{period } 2T: \mathbf{a} = \sum_{k=1,3,\ldots}^{\infty} \left(\mathbf{c}_k \sin \frac{k\omega t}{2} + \mathbf{d}_k \cos \frac{k\omega t}{2} \right),$$

$$\text{period } T: \mathbf{a} = \tfrac{1}{2}\mathbf{d}_0 + \sum_{k=2,4,\ldots,}^{\infty} \left(\mathbf{c}_k \sin \frac{k\omega t}{2} + \mathbf{d}_k \cos \frac{k\omega t}{2} \right). \tag{30}$$

If the series expansions of equation (30) are used in equation (28), term-wise comparisons of the sine- and cosines coefficients will give infinite systems of homogeneous algebraic

equations for the vectors $\mathbf{c}_k$ and $\mathbf{d}_k$ for the solutions on the stability borders. Non-trivial solutions exist if the determinant of the coefficient matrices of these equation systems of infinite order vanish. When looking for numerical solutions, systems of finite order are required and as it is shown in reference [6], a sufficiently close approximation of the infinite eigenvalue problems is obtained by taking $k = 1, 2$ in the expansions in equation (30) and putting the determinants of the coefficient matrices of the first order equal to zero (see also reference [8]).

4.1. PERIOD 2T

Using the first order time series expansion of equation (30) in equation (28) the following determinant is achieved:

$$\left| \begin{bmatrix} \mathbf{K}^{sum} - \frac{1}{2}\mu(E + \bar{E})\mathbf{K}_{gD} & \mathbf{0} \\ \mathbf{0} & \mathbf{K}^{sum} + \frac{1}{2}\mu(E + \bar{E})\mathbf{K}_{gD} \end{bmatrix} + \begin{bmatrix} \mathbf{0} & \frac{1}{2}(\frac{1}{2}\mathbf{K}_{gD} - \mathbf{C}^{sum}) \\ \frac{1}{2}(\frac{1}{2}\mathbf{K}_{gD} + \mathbf{C}_{sum}) & \mathbf{0} \end{bmatrix}\omega + \begin{bmatrix} -\frac{1}{4}\mathbf{M} & \mathbf{0} \\ \mathbf{0} & -\frac{1}{4}\mathbf{M} \end{bmatrix}\omega^2 + \begin{bmatrix} \mathbf{0} & \frac{1}{8}\mathbf{M}^* \\ -\frac{1}{8}\mathbf{M}^* & \mathbf{0} \end{bmatrix}\omega^3 \right| = 0, \tag{31}$$

where

$$\mathbf{K}^{sum} = \mathbf{K}_e + \mu(E + \bar{E})\mathbf{K}_{gS},$$

$$\mathbf{C}^{sum} = \mathbf{K}_{gS} + \mathbf{C}. \tag{32}$$

To solve the third order eigenvalue equation of the system of equation (31) a standard transformation is needed. Consider a general matrix equation of third order in ω written in standard form, i.e.

$$(\mathbf{A}_0 + \omega\mathbf{A}_1 + \omega^2\mathbf{A}_2 + \omega^3\mathbf{A}_3)\mathbf{X} = \mathbf{0}, \tag{33}$$

where $\mathbf{A}_0, \mathbf{A}_1, \mathbf{A}_2, \mathbf{A}_3$ are square matrices, all of the same order and $\mathbf{X}$ is some eigenvector. An enlarged eigenvector $\mathbf{U}$ is introduced as

$$\mathbf{U} = \begin{bmatrix} \mathbf{X} \\ \omega\mathbf{X} \\ \omega^2\mathbf{X} \end{bmatrix}. \tag{34}$$

By use of this enlarged eigenvector, the third order eigenvalue problem in equation (33) is transformed to a linear one,

$$\left| \begin{bmatrix} \mathbf{A}_0 & \mathbf{0} & \mathbf{0} \\ \mathbf{0} & \mathbf{I} & \mathbf{0} \\ \mathbf{0} & \mathbf{0} & \mathbf{I} \end{bmatrix} - \omega \begin{bmatrix} -\mathbf{A}_1 & -\mathbf{A}_2 & -\mathbf{A}_3 \\ \mathbf{I} & \mathbf{0} & \mathbf{0} \\ \mathbf{0} & \mathbf{I} & \mathbf{0} \end{bmatrix} \right| = 0, \tag{35}$$

which can be solved with standard methods. When applying this transformation in equation (31) it is noted that if the original matrices $\mathbf{K}_e$, $\mathbf{K}_{gS}$, $\mathbf{K}_{gD}$, $\mathbf{C}$, $\mathbf{M}$ and $\mathbf{M}^*$ are of order $(n \times n)$, then the third order expression of equation (31) is of order $(2n \times 2n)$ and the transformed generalized eigenvalue problem, which has to be solved, is of order $(6n \times 6n)$.

Solving the eigenvalue problem of equation (31) will give an approximation of the principal region of stability where the solutions on the stability borders have the time period $2T$.

4.2. PERIOD T

When the second time series expansion of equation (30) is used in equation (28) the following determinant is achieved:

$$\left| \begin{bmatrix} \mathbf{K}^{sum} & \mathbf{0} \\ \mathbf{0} & \mathbf{K}^{sum} - \mathbf{K}^{inv} \end{bmatrix} + \begin{bmatrix} \mathbf{0} & (\mathbf{K}^{inv} - \mathbf{C}^{sum}) \\ \mathbf{C}^{sum} & \mathbf{0} \end{bmatrix} \omega + \begin{bmatrix} -\mathbf{M} & \mathbf{0} \\ \mathbf{0} & -\mathbf{M} \end{bmatrix} \omega^2 + \begin{bmatrix} 0 & \mathbf{M}^* \\ -\mathbf{M}^* & 0 \end{bmatrix} \omega^3 \right| = \mathbf{0}, \tag{36}$$

where

$$\mathbf{K}^{inv} = \mathbf{K}_{gD}(\mathbf{K}_e + \mu(E + \bar{E})\mathbf{K}_{gS})^{-1}\tfrac{1}{2}\mathbf{K}_{gD}. \tag{37}$$

The solution of the eigenvalue problem of equation (36) by the transformation method described above gives the secondary instability region which has border lines with periodic solutions of periodicity T.

5. NUMERICAL RESULTS

The calculations were performed in Matlab [15] with use of the finite element toolbox CALFEM [10] and the procedure was as follows. In the initialization phase the geometry and material parameters were specified. The elements in use were standard beam elements and the problem had 15 degrees of freedom. The value of the static loading has been set to zero, i.e., $P_S = 0$ in all the presented investigations. The dynamic load, P_D, was increased stepwise and for each value of the dynamic load, all matrices in equations (31) and (36) were calculated, the eigenvalue problem was solved and frequencies at the stability boundaries were obtained. The results for the undamped simply supported system are presented in Figure 3.

To obtain information about the influence of the material damping, systematic investigations were performed of the simply supported system. The value of the two material parameters $\bar{E}$ and μ were varied and the location of the principal instability region was followed. From Figure 4 (left), where $\mu =$ constant and $\bar{E}$ is varied, it can be concluded that the position of the instability region moves and opens up when $\bar{E}$ decreases (when $\bar{E} = 0$, a Maxwell material is achieved). It appears that the lowest value of the amplitude for which instability occurs moves along the dash-dotted curve ABC as $\bar{E}$ is decreased.

The corresponding behaviour for decreasing values of μ and keeping $\bar{E}$ constant is shown in Figure 4 (right). Here the stability region moves to decreasing values of frequencies and

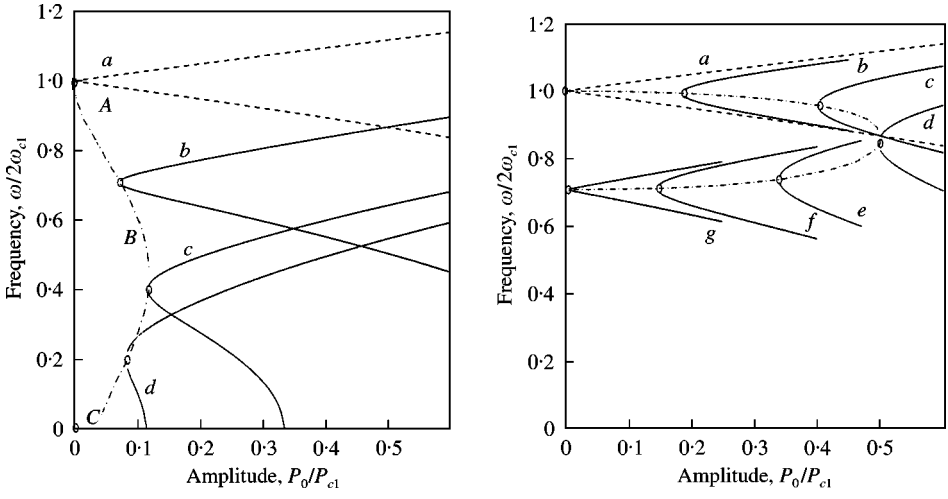

Figure 4. Stability chart. The left chart shows the influence of varying $\bar{E}$ when $\mu = 2{\cdot}1 \times 10^{-9}\,\mathrm{m^2/N\,s}$ and in the right chart μ is varying when $\bar{E} = 100E = 2{\cdot}1 \times 10^{13}\,\mathrm{N/m^2}$. (A) (a) $\bar{E} = 100\bar{\mathrm{E}}$, (b) $\bar{E} = \mathrm{E}$, (c) $\bar{E} = 0{\cdot}2\mathrm{E}$, (d) $\bar{E} = 0{\cdot}06\mathrm{E}$; (B) (a) $\mu = 0$, (b) $\mu = 0{\cdot}042 \times 10^{-9}\,\mathrm{m^2/N\,s}$, (c) $\mu = 0{\cdot}11 \times 10^{-9}\,\mathrm{m^2/N\,s}$, (d) $\mu = 0{\cdot}21 \times 10^{-9}\,\mathrm{m^2/N\,s}$, (e) $\mu = 0{\cdot}42 \times 10^{-9}\,\mathrm{m^2/N\,s}$, (f) $\mu = 1{\cdot}1 \times 10^{-9}\,\mathrm{m^2/N\,s}$, (g) $\mu = 210 \times 10^{-9}\,\mathrm{m^2/N\,s}$.

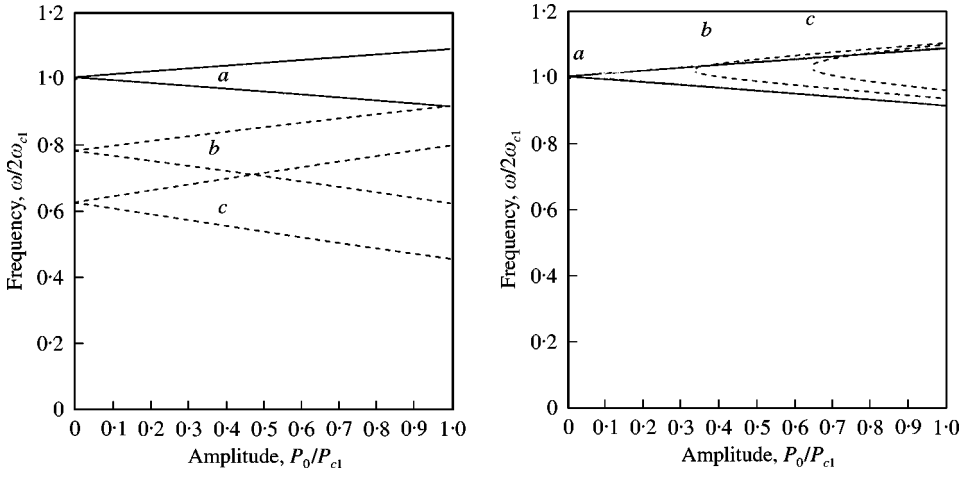

Figure 5. Calculations of a clamped–simply supported system with no material damping and, presented in the left chart, different values of k_b, i.e., varying the stiffness in the hinge while $c_b = 0$ (constant), and in the right chart different values of c_b, i.e., varying the damping in the hinge while $k_b = 0$ (constant). (A) (a) $k_b = 0$, $c_b = 0$; (b) $k_b = 12\,\mathrm{N/m}$, $c_b = 0$; (c) $k_b = 13\,\mathrm{N/m}$, $c_b = 0$; (B) (a) $k_b = 0$, $c_b = 0$; (b) $k_b = 0$, $c_b = 0{\cdot}02\,\mathrm{N\,m/s}$; (c) $k_b = 0$, $c_b = 0{\cdot}03\,\mathrm{N\,m/s}$.

the lowest value of the load amplitude to reach instability first increases and then decreases when the value of μ increases.

In Figure 5, the influence of the two parameters governing damping in the boundary conditions, k_b and c_b, is investigated. The conclusion of this investigation is that varying k_b will move the principal instability region in the vertical direction only (Figure 5 (left)) while, on the other hand, by increasing c_b the instability region is moved primarily in the horizontal direction (Figure 5 (right)).

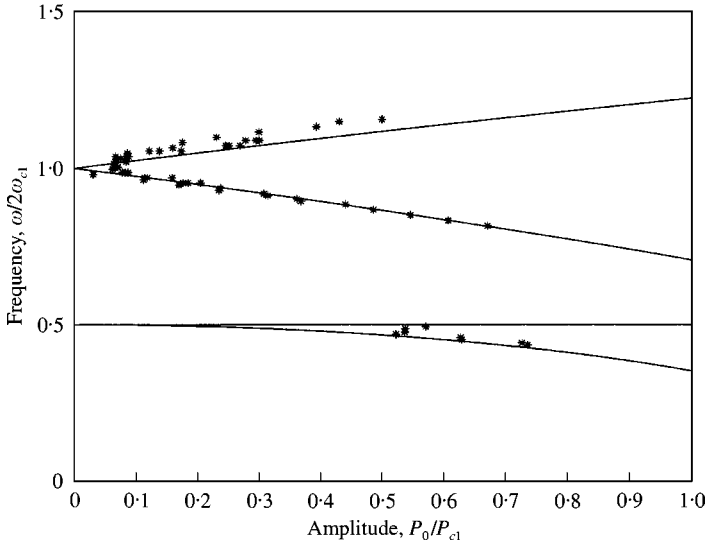

Figure 6. Stability chart for the simply supported steel beam. The stars represent experimental data and the solid lines denote results from calculations for linear elasticity (i.e., $\mu = 0$).

6. EXPERIMENTAL RESULTS

The influence of material damping and damping in the hinges will now be investigated experimentally and comparisons with simulations will be presented.

The experimental set-up can be described as a horizontally oriented beam with hinges at both ends. One of the hinges is connected to an electro-magnetic vibrator and the other to a load cell. A more detailed description of the set-up is presented in reference [4]. It should be noted that the constraints for the midpoint deflection of the beam that are described in reference [4] are not used in the work presented here.

The loading points on the periodic border lines between stable and unstable motions were experimentally detected as follows: for each frequency of interest and a low load amplitude level, the beam midpoint was given an initial deflection and velocity and it was observed that the lateral vibrations fade out. This procedure was repeated at increasing levels of load amplitudes until the lateral vibration became periodic; this periodicity signals the instability border.

The investigation was first carried out with a beam made of steel with a cross-section of $1 \times 25\ \text{mm}^2$ and a length of 400 mm. This gives the first buckling load as 25 N and the first eigenfrequency as 14 Hz which has been used for normalization of the experimental results presented in Figure 6. In the corresponding simulations, no damping effects were considered and it appears that a close agreement between experimental data and simulations was obtained.

To capture material damping, a glass-mat-reinforced thermoplastic material (GMT) was chosen. The GMT beam had a first buckling load of 39 N and a lowest eigenfrequency of 23 Hz. The experimental results are presented in Figure 7 and the damping is obvious. The dashed curves in Figure 7 are obtained from calculations with material damping, i.e., $\bar{E} = 3E$ (where $E = 6 \times 10^9\ \text{N/m}^2$) and $\mu = 9{\cdot}0 \times 10^{-13}\ \text{m}^2/\text{N s}$ as well as $k_b = c_b = 0$. The close agreement between experimental data and simulations proves that the damping effects, indeed, are due to material damping alone. This conclusion is supported by comparisons with the effects of material damping and hinge damping illustrated in

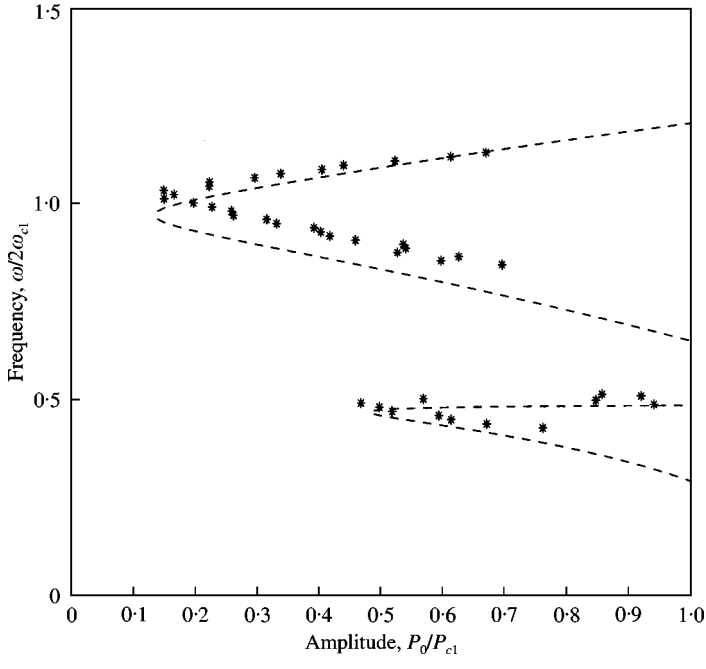

Figure 7. Stability chart for the glass-mat-reinforced thermoplastic simply supported beam. The stars denote experimental data and the dashed lines represent results from calculations with the material parameters, $E = 6 \times 10^9$ N/m^2, $\bar{E} = 3E$ and $\mu = 9{\cdot}0 \times 10^{-13}$ m^2/N s.

Figures 4 and 5 respectively. It is concluded that damping in the hinges in the present experimental set-up is quite small.

To obtain experimental data for damping in the hinges, advantage is taken of the study presented in reference [9]. The response of a steel beam (clamped–simply supported) was investigated and a quite substantial discrepancy between their simulations and experimental data was observed. It will be shown here that very accurate predictions can be obtained if damping in the hinge is considered. The experimental data of reference [9] are shown in Figure 8 and since the material is steel, material damping can be ruled out (Figure 6).

Simulations with various values for the hinge damping parameters were performed and best agreement with experimental results was obtained with $c_b = 300$ N m/s, $k_b = 10{\cdot}8$ N m for the hinge at the simply supported end. These simulations are also shown in Figure 8 and close agreement is obtained with the experimental data.

7. CONCLUSIONS

An accurate numerical method for investigation of the stability properties of a dynamic system with periodic coefficients has been presented. Both internal damping and damping at the boundaries of the system can be accounted for. The actual differential equations do not have to be solved; instead, the stability boundaries are approximated by solving an eigenvalue problem which has been derived by Fourier expansion.

Due to the starting point of a quite general material model in terms of a standard material model, third order time derivatives are present in the governing equations. This fact does

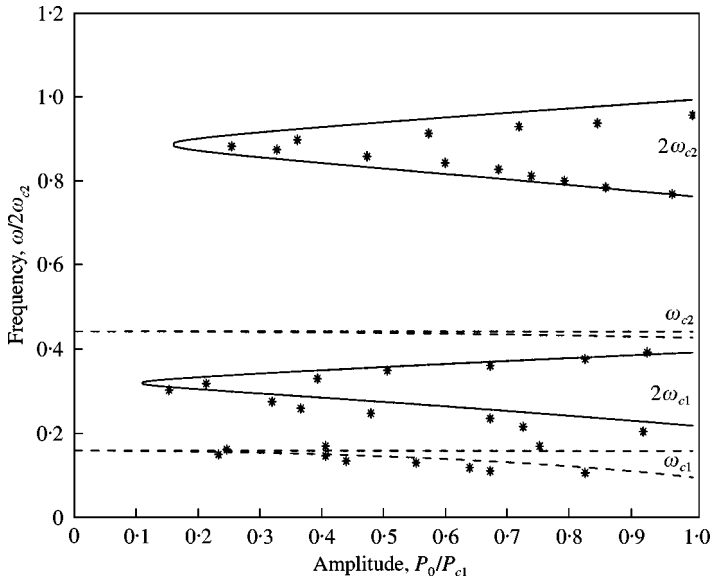

Figure 8. Stability chart of a clamped–simply supported steel beam. The stars denote experimental data from reference [15] and the solid and dashed lines represent results from calculations with the hinge parameters $c_b = 300$ N m/s and $k_b = 10{\cdot}8$ N m.

not affect the use of the Floquet solution and the interpretation of the stability problem, which being an eigenvalue problem, is solvable with standard methods.

The material model is able to capture a variety of material behaviours and a close correspondence is reached for calculated values and the experimental data from the present set-up with materials with and without damping. Moreover, with the damping model of the hinges it is possible to explain experimental data found in the literature.

REFERENCES

1. R. PANDIYAN and S. C. SINHA 1995 *Nonlinear Dynamics* **8**, 21–43. Analysis of time-periodic nonlinear dynamical systems undergoing bifurcations.
2. S. W. SHAW and R. H. RAND 1989 *International Journal of Non-Linear Mechanics* **24**, 41–56. The transition to chaos in a simple mechanical system.
3. J.-D. JIN and Y. MATSUZAKI 1988 *Journal of Sound and Vibration* **126**, 265–277. Bifurcations in a two-degree-of-freedom elastic system with follower forces.
4. I. SVENSSON 1996 *Nonlinear Dynamics* **11**, 315–328. Dynamic buckling of a beam with transverse constraints.
5. P. FRIEDMANN and C. E. HAMMOND 1977 *International Journal of Numerical Methods in Engineering* **11**, 1117–1136. Efficient numerical treatment of periodic systems with application to stability problems.
6. V. V. BOLOTIN̄ 1964 *The Dynamic Stability of Elastic Systems*. San Francisco: Holden-Day.
7. K. G. LINDH and P. W. LIKINS 1970 *American Institute of Aeronautics and Astronautics Journal* **8**, 680–686. Infinite determinant methods for stability analysis of periodic-coefficient differential equations.
8. W. B. KRÄTZIG and L.-Y. LI 1992 *International Journal of Solids Structures* **29**, 97–104. On rigorous stability conditions for dynamic quasi-bifurcations.
9. T. IWATSUBO M. SAIGO and Y. SUGIYAMA 1973 *Journal of Sound and Vibration* **30**, 65–77. Parametric instability of clamped–clamped and clamped–simply supported columns under periodic axial load.

10. Division of Structural Mechanics and Division of Solid Mechanics, LTH, Lund University. *CALFEM*, *A fine element toolbox to MATLAB*, *version* 3.2, October 1995.
11. Y. C. FUNG 1965 *Foundations of Solid Mechanics*. Englewood Cliffs, NJ: Prentice-Hall.
12. J. LEMAITRE and J.-L. CHABOCHE 1990 *Mechanics of Solid Materials*. Cambridge: Cambridge University Press.
13. N. W. LACHLAN 1964 *Theory and Application of Mathieu Functions*. New York: Dover Publ.
14. G. IOOSS and D. D. JOSEPH 1990 *Elementary Stability and Bifurcation Theory*. New York: Springer-Verlag; second edition.
15. *Matlab Reference Guide*, August 1992.